https://doi.org/10.5194/egusphere-2025-5460
Preprint. Discussion started: 24 November 2025

Fault-Controlled Distribution of Pre-seismic Thermal Anomalies: Insights from the Dingri Earthquakes, Tibet

Wanyi Li[1,2], Dan Tao[1,2], Jiufeng Wang[1,2], Xiang Wei[1,2], Qianxi Zhang[1,2], Yinqian Li[1,2], Sirui Li[1,2], Huaxiang Qin[1,2], and Qifeng Jiang[1,2]

[1]Key Laboratory of Earth Exploration and Information Techniques of Ministry of Education, Chengdu University of Technology, Chengdu, 610059, China
[2]College of Geophysics, Chengdu University of Technology, Chengdu, 610059, China

Correspondence: Dan Tao (dan.tao@cdut.edu.cn)

Abstract. This study analyzed pre-seismic thermal anomalies associated with two earthquakes in Tibet's Tingri region using MODIS data processed via STL (Seasonal-Trend decomposition using LOESS) decomposition and RST (Robust Satellite Techniques) algorithm. The results reveal relatively prominent thermal anomalies within the study area during the six months preceding the earthquake occurrences. Spatially, these thermal anomalies exhibited distinctly fault-aligned distributions, particularly near the seismogenic structure (Dingmu Co fault) and major regional structures (Himalayan orogenic belt). The distribution of thermal anomalies was significantly aligned with the orientations of the faults, supported by fitting and translation analyses. Quantitative correlations exceeded 0.99 (Dingmu Co fault) and 0.95 (the Himalayan orogenic belt), indicating exceptionally strong linear relationships. These findings suggest that thermal anomalies are intrinsically linked to fault activity and may serve as potential earthquake precursors. Furthermore, time series analysis (2016-2025, Ms≥4.0) further confirmed the correlation between thermal anomaly indices and the timing of seismic events, supporting their predictive value. However, unresolved issues, such as the intervals between anomaly peaks and seismic events, and the universality of spatial correlations, require further investigation to refine earthquake prediction frameworks.

1 Introduction

Earthquakes are natural phenomena that occur within the Earth's crust. The preparation process for an earthquake begins with the accumulation of elastic strain, and when the elastic strain in rocks reaches its limit, it leads to sudden fault rupture and the release of elastic energy, resulting in an earthquakeReid (1910); Scholz (2002); Rogers and Dragert (2003). This rapid release of energy not only poses a severe threat to human society but also has a profound impact on the natural environment Bayram et al. (2023); Hill et al. (2024). Due to their unpredictability, earthquakes have always been a topic of widespread interest among experts and scholars Geller et al. (1997); Panda et al. (2007); Koronovskii et al. (2021). Since the 1980s, when researchers began to explore thermal anomalies associated with earthquakes, it has gradually been recognized that infrared remote sensing

https://doi.org/10.5194/egusphere-2025-5460
Preprint. Discussion started: 24 November 2025

technology has unique advantages in earthquake monitoring and prediction Saraf et al. (2008); Hassini and Belbachir (2014); Jiang et al. (2025). Gorny et al. (1988) first proposed that thermal infrared radiation at fault intersections increases before most moderate to strong earthquakes in Central Asia, providing a new perspective for earthquake prediction. With the development of technology and the deepening of research, more pre-earthquake thermal infrared anomalies have been discovered Rawat et al. (2011); Yao and Qiang (2012); Liu et al. (2016); Kancherla et al. (2018). These observed thermal infrared anomalies can be explained by several mechanisms. Specifically, thermal anomalies are commonly interpreted as (1) the release of various greenhouse gases in the Earth's crust, such as CO_2, N_2O, and CH_4 Tronin et al. (2002); Choudhury et al. (2006); Saraf (2008); Jiao et al. (2017); (2) the p-hole activation mechanism Freund et al. (2006, 2007); Freund (2011); (3) friction from rock rupture Wu et al. (2006); Cicerone et al. (2009); Allison and Dunham (2020); Liu et al. (2022); (4) the coupling effect of multiple spheres Pulinets et al. (2006); Jing et al. (2019); Marchetti et al. (2019); Ghamry et al. (2021); De Santis et al. (2022). Multiple methods exist for detecting pre-earthquake thermal anomalies, such as Robust Satellite Techniques (RST), wavelet transform, interquartile range method, and filtering change analysis. Saradjian and Akhoondzadeh (2011); Tramutoli (2015); Zhang and Meng (2019); Lai et al. (2023); Wu et al. (2023b). Building upon these established foundations concerning the mechanisms, detection methods, and the critical link between thermal anomalies and fault dynamics, this study advances earthquake precursor research by addressing key unresolved challenges. While spatial correlations and fault-distance frameworks exist Wei et al. (2013); Karimi Zarchi and Saradjian Maralan (2020), quantitative characterization of the intrinsic relationship between specific fault structures and the spatiotemporal evolution of thermal anomalies remains underexplored, particularly for moderate events in complex terrains like Tibet. Furthermore, despite the availability of MODIS LST data Panda et al. (2007) and techniques like RST Tramutoli (2015), effectively isolating subtle seismic-related signals from persistent seasonal noise in long-term time-series requires enhanced methodologies.

To address these gaps, this study utilized MODIS-derived Land Surface Temperature (LST) products (1 January 2016 – 9 February 2025) and innovatively integrated the Seasonal-Trend decomposition using Loess (STL) method with the Robust Satellite Techniques (RST) algorithm to minimize seasonal interference. This approach enabled an in-depth analysis of spatiotemporal characteristics of thermal anomalies associated with the Dingri earthquakes in Tibet, generating distribution maps and evolutionary time-series plots. The research then focused on regions with pronounced thermal anomalies proximal to active faults, subjecting the data to fitting and spatial shift analysis. Additionally, we introduced correlation coefficients to quantitatively characterize the fault-thermal anomaly relationship—a novel advancement toward objective validation. Additionally, time-series analysis of thermal anomaly indices for Ms$\geq$4.0 events (2016–2025) provided new insights into precursor signals for moderate earthquakes. These findings deliver critical insights and novel perspectives for earthquake prediction research, establishing a valuable reference for investigating seismic thermal anomalies in Dingri and surrounding regions.

https://doi.org/10.5194/egusphere-2025-5460
Preprint. Discussion started: 24 November 2025

2 Study Area Overview and Data Sources

2.1 Earthquake Basic Parameters and Study Area Overview

This study designates the 20 March 2020 Ms5.9 Dingri earthquake (epicenter: 28.63°N, 87.42°E) in Tibet as the primary research focus. A 5°×5° region centered on the epicenter was selected as the study area, utilizing seismological parameters from the China Earthquake Networks Center (CENC; Figure 1). The seismogenic structure is identified as Dingmu Co Fault, a subsidiary structure of the Shenzha-Dingjie Fault Zone along the southeastern margin of the Lhasa Block Zhang et al. (2020); Li et al. (2024); Jin et al. (2025). This fault exhibits a near-N-S strike, westerly dip, and normal fault kinematics. Geodynamically, the Tibetan Plateau occupies the collision front of the ongoing India-Eurasia continental collision. Under continued northward subduction of the Indian Plate and compressional stresses from the Eurasian Plate, the region has developed a dominant E-W-oriented extensional stress regime, generating systematic N-S-trending normal fault systems. This tectonic configuration establishes the study area as one of the most seismically active zones in southern Tibet, with 738 recorded earthquakes occurring between 2000 and 1 March 2025 (including 76 events with Ms≥5.0 and 6 events with Ms≥6.0). To validate methodological robustness within this tectonic framework, we also conducted a comparative analysis of an assumed co-tectonic earthquake occurring on 7 January 2025, while maintaining the 2020 event as the principal demonstrative case. Collectively, these manifestations of seismicity underscore the region's significance within southern Tibet's seismic hazard profile, providing critical empirical constraints for characterizing regional tectonics and seismic potential.

3 Data Sources

The Moderate Resolution Imaging Spectroradiometer (MODIS), a NASA-developed Earth observation instrument aboard the Terra (1999) and Aqua (2002) polar-orbiting satellites, has served as a cornerstone of global environmental monitoring. Providing multispectral data with high temporal resolution, MODIS observations are widely applied in meteorological, climatological, and ecological research. This study employs the MOD11A2 product—an 8-day composite dataset derived from daily MOD11A1 acquisitions—featuring 1-km spatial resolution per 1200×1200 km scene.

4 Data Processing Methods

4.1 STL Time Series Decomposition Method

STL (Seasonal and Trend decomposition using LOESS) is a time-series-decomposition method proposed by Cleveland et al. (1990). It decomposes a time series into trend, seasonal, and remainder components.

$$\text{Remainder}(x,y,t) = Y(x,y,t) - \text{Trend}(x,y,t) - \text{Seasonal}(x,y,t) \quad (1)$$

Here, Remainder(x,y,t), Y(x,y,t), Trend(x,y,t), and Seasonal(x,y,t) represent the remainder, observed value, trend, and seasonal components at location (x,y) and time t, respectively. The trend component reflects long-term, low-frequency changes; the

https://doi.org/10.5194/egusphere-2025-5460
Preprint. Discussion started: 24 November 2025

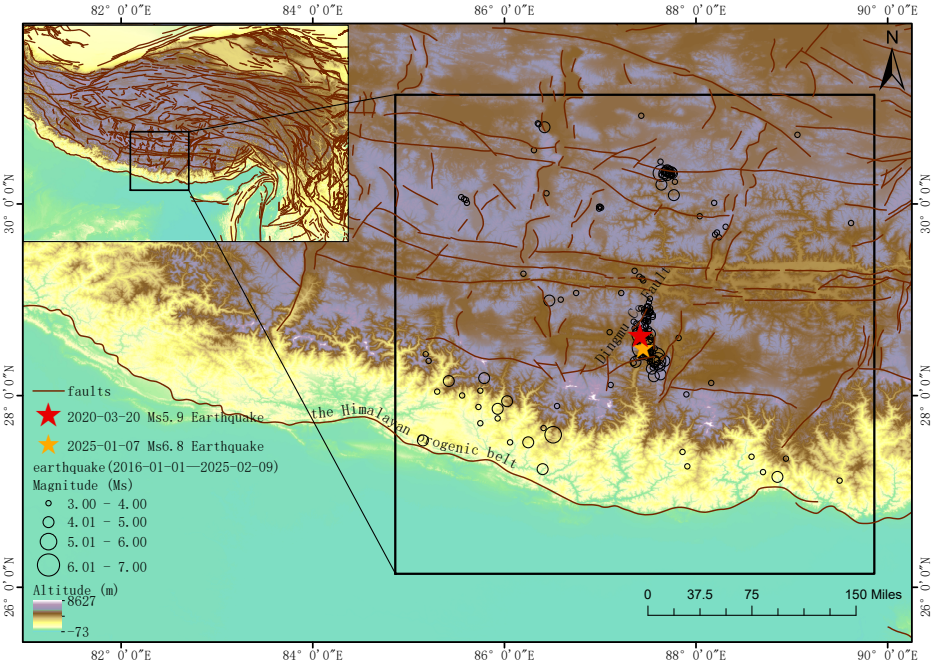

Figure 1. Distribution Map of Seismic Activity, Faults and Topographic Features in Dingri, Tibet (The area in the box is the study area, including Dingmu Co Fault and the Himalayan orogenic belt. The red pentagram represents the Ms5.9 earthquake on March 20, 2020, and the orange pentagram represents the Ms6.8 earthquake on 7 January 2025. The black circles in different sizes indicate the earthquakes from 1 January 2016 to 9 February 2025.)

seasonal component indicates medium-frequency, regular fluctuations; and the remainder component captures high-frequency, irregular variations. STL is a systematic approach that extracts these components through inner and outer loops. The inner loop focuses on trend fitting and periodic-component calculations, while the outer loop adjusts robust weights to enhance the decomposition's robustness. In each inner loop, three LOESS (locally weighted regression) smoothings and a moving average are applied. LOESS assumes stronger correlations over shorter distances and performs local weighted regression by selecting window length, weight function, and regression-equation order. The three LOESS smoothings are used for period-subseries smoothing (extracting seasonal components), low-pass filtering (extracting trend components), and trend smoothing (refining trend components). This study successfully constructed a spatiotemporal dataset of residual terms using equation (1), and the detailed operation process is shown in Figure 2.

4.2 The RST Algorithm

The RST (Robust Satellite Techniques) method, introduced by Tramutoli (1998), was first applied to the detection of seismic infrared anomalies in 2001. This technique, based on the analysis of multi-temporal satellite data, constructs a background field by analyzing long sequences of satellite data and calculates the local deviation index to identify anomalies under quiescent

https://doi.org/10.5194/egusphere-2025-5460
Preprint. Discussion started: 24 November 2025

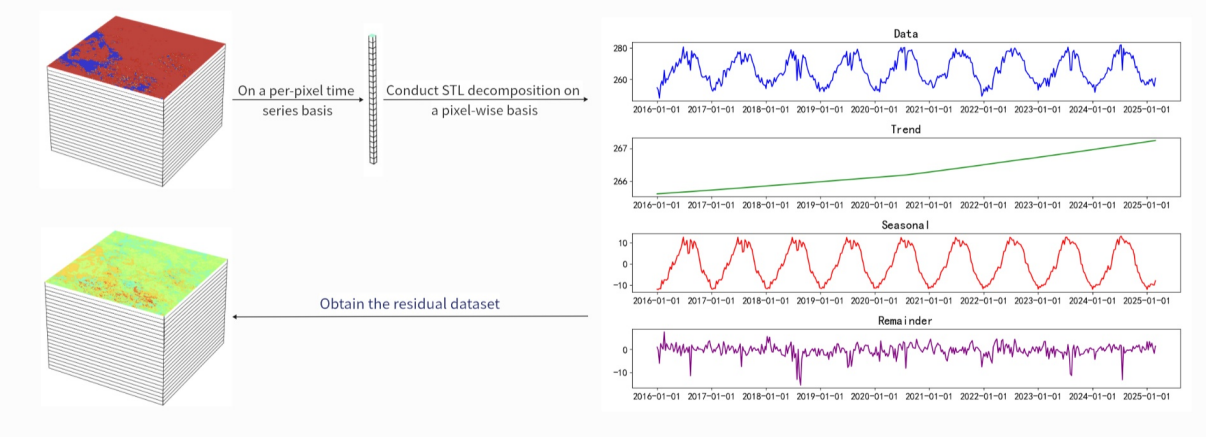

Figure 2. STL-Based Seismic Thermal Anomaly Decomposition Process (Decompose raster data into pixel-time series groups, perform STL decomposition on each group, extract trend, seasonal and residual components from time series. Remove trend and seasonal components from original data, then merge each group to obtain the residual dataset.)

conditions.

$$\text{Alice}(x,y,t) = \frac{Y(x,y,t) - \mu(x,y,t)}{\sigma(x,y,t)} \tag{2}$$

$$\mu(x,y,t) = \frac{1}{N}\sum_{i=1}^{N} T_i(x,y,t) \tag{3}$$

$$\sigma(x,y,t) = \sqrt{\frac{1}{N}\sum_{i=1}^{N}\left(T_i(x,y,t) - \mu(x,y,t)\right)^2} \tag{4}$$

where: $\text{Alice}(x,y,t)$ is the anomaly value at location (x,y) and time t. $Y(x,y,t)$ is the observed value at location (x,y) and time t. $\mu(x,y,t)$ is the average value calculated from multi-year data at the same time t and location (x,y), serving as a background field. $\sigma(x,y,t)$ is the standard deviation derived from the background field.

The background field can mitigate errors caused by natural factors, thereby enhancing the precision of earthquake anomaly extraction. The RST algorithm leverages the expected value (multi-year average) and variability (multi-year standard deviation) from long-term observational datasets to characterize anomalies in the measured signal. By integrating neighborhood differencing with background field normalization, it defines a mathematical expression for pre-earthquake anomalies in statistics. Through the specific index $\text{Alice}(x,y,t)$, the RST method effectively identifies thermal infrared anomalies, In general, an anomaly is defined as occurring when the anomaly index I exceeds 2, i.e., $I > 2$.

In this study, the RST algorithm was applied to the residual components obtained from STL decomposition. This integrated approach maximizes the reduction of seasonal interference in the data, thereby enhancing the specificity of seismic thermal anomaly extraction.

https://doi.org/10.5194/egusphere-2025-5460
Preprint. Discussion started: 24 November 2025

5 Analytical Studies

5.1 Spatiotemporal Evolution of Thermal Anomalies

This study applied Seasonal-Trend decomposition using Loess (STL) to MOD11A2 data (1 January 2016 to 9 February 2025) and employed Robust Satellite Techniques (RST) for residual anomaly detection, generating spatiotemporal thermal anomaly maps for the Ms5.9 Dingri earthquake (20 March 2020; Figure 3). Key findings revealed distinct thermal evolution phases: During 14 September to 15 October 2019, scattered low-intensity anomalies indicated initial crustal stress accumulation without significant epicentral anomalies. From 16 to 31 October 2019, expanding anomalies with enhanced intensity reflected concentrated crustal stress and increased fault activity. Subsequently during 1 to 16 November 2019, anomalies reached peak intensity and spatial extent, signifying progressive stress accumulation accompanied by rock fracturing processes-potentially representing precursory signals-with distinct spatial patterns correlated with faults along Dingmu Co Fault and the Himalayan orogenic belt requiring further investigation. From 17 November to 2 December 2019, anomalies diminished while remaining fault-concentrated, suggesting stress release or thermal diffusion. Minimal thermal activity occurred from 3 December 2019 to 21 March 2020, except for scattered anomalies during 10 to 17 February 2020, likely indicating stress redistribution. Post-seismic thermal anomalies emerged during 22 to 29 March 2020, indicating delayed heat propagation from co-seismic ruptures, with no detectable anomalies observed thereafter until 22 April 2020.

5.2 Temporal Variation of Thermal Anomalies

Figure 4 depicts the temporal variations in thermal anomaly pixel counts from 14 September 2019 to 15 April 2020, compared with the average values from non-seismic years during the same period. Pronounced fluctuations are observed throughout the six-month pre-seismic and one-month post-seismic intervals. From September to mid-October 2019, pixel counts remained consistently low, aligning closely with the multi-year average. Beginning on 16 October 2019, counts increased progressively, reaching a peak of 510,000 pixels on 1 November—substantially higher than the non-seismic average and indicating a strong pre-seismic anomaly signal. Subsequently, values declined over approximately 47 days, returning to normal levels while retaining detectable anomalies during the transition. Between 3 December 2019 and the mainshock on 20 March 2020, only one minor fluctuation was recorded. A subtle post-seismic fluctuation was also observed. This temporal pattern corresponds closely with the observed spatiotemporal anomaly characteristics. Notably, the earthquake occurred 140 days after the thermal anomaly peak on 1 November 2019.

5.3 Geospatial Coupling of Seismogenic Faults and Thermal Anomalies

Earthquakes may result from elastic energy transfer within active fault zones proximal to epicentersAlvan et al. (2013). Analysis in Section 4.1 revealed significant spatial correlations between thermal anomalies and major tectonic structures, particularly along Dingmu Co Fault and the Himalayan orogenic belt. To empirically validate relationships between pre-seismic thermal enhancement and fault activity, we systematically analyzed thermal anomaly distributions relative to fault strike orientations.

https://doi.org/10.5194/egusphere-2025-5460
Preprint. Discussion started: 24 November 2025

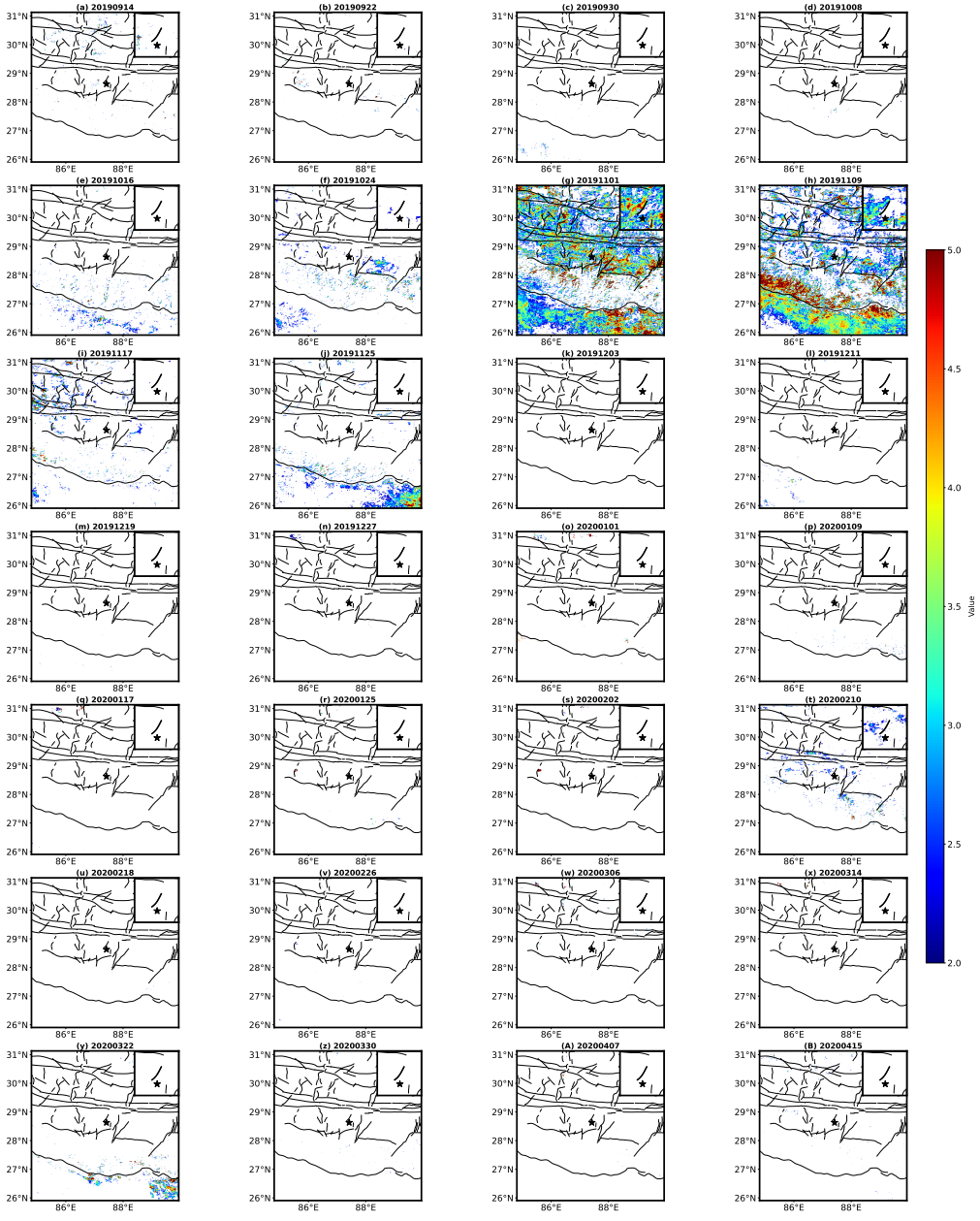

Figure 3. Spatiotemporal Distribution of Thermal Anomalies with the 20 March 2020 Ms5.9 Dingri Earthquake, Tibet (Twenty-eight thermal anomaly heatmaps generated for eight-day compositing periods spanning six months pre-seismic to one month post-seismic. Subplot titles (e.g., "20190914") denote the start date of each composite period (e.g., 14-21 September 2019). Insets (upper-right) detail anomalies along the seismogenic Dingmu Co Fault zone. Colorbar indicates anomaly intensity (blue = 2.0 to red = 5.0), with values <2.0 masked and >5.0 saturated at 5.0.)

https://doi.org/10.5194/egusphere-2025-5460
Preprint. Discussion started: 24 November 2025

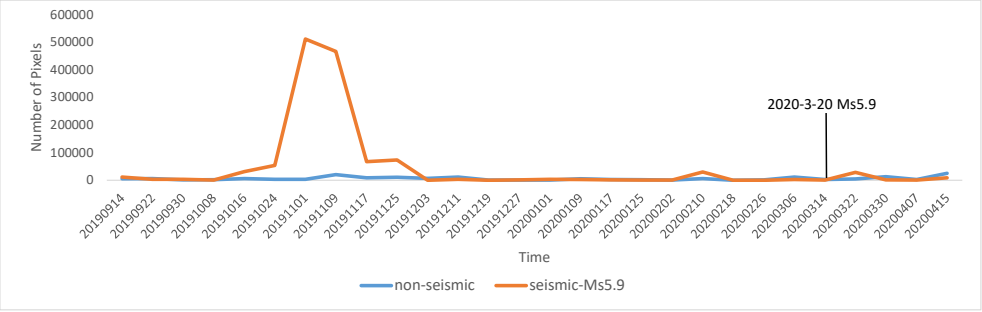

Figure 4. Temporal evolution of thermal anomalies: Ms5.9 Dingri earthquake, Tibet (20 March 2020) (The orange line represents the variation in the number of anomalous pixels during the period from six months before the earthquake to one month after its occurrence, while the blue line indicates the corresponding variation in the average number of anomalous pixels during the same time interval in selected non-seismic years.)

Figure 5 illustrates spatial relationships between Dingmu Co Fault and fitted thermal anomaly curves. On 1 November 2019, anomalies predominantly clustered northwest of the fault with peak intensities concentrated along its central segment. On 9 November 2019, while maintaining northwestward concentration, anomalies exhibited higher magnitudes in the southwestern sector compared to the northeastern zone. We derived fitting curves from thermal anomaly distributions and implemented minimum-distance optimization to determine translational parameters minimizing cumulative distance between curves and fault trace. Post-optimization results demonstrate striking alignment between translated curves and Dingmu Co Fault, both exhibiting near N-S strikes. Pearson Correlation Coefficients (PCC) were computed to quantify relationships between thermal anomalies and fault geometry:

$$r = \frac{\sum_{i=1}^{n}(x_i - \bar{x})(y_i - \bar{y})}{\sqrt{\sum_{i=1}^{n}(x_i - \bar{x})^2}\sqrt{\sum_{i=1}^{n}(y_i - \bar{y})^2}} \tag{5}$$

Here, x_i and y_i are sample data of thermal infrared anomalies and fault characteristics, respectively. $\overline{x}$ and $\overline{y}$ are their means, and n is the sample size. This coefficient evaluates the strength and direction of the linear relationship between two variables. If the value is close to 1, it means a strong positive correlation; if close to -1, a strong negative correlation; and if close to 0, it indicates no obvious linear correlation. The Pearson correlation coefficients calculated between thermal anomalies and Dingmu Co Fault were exceptionally high (0.9980 and 0.9957), confirming a near-perfect positive linear correlation. Beyond this specific seismogenic structure, similar thermal anomalies were observed along the broader the Himalayan orogenic belt. Figure 6 illustrates the spatial relationship between the Himalayan orogen and its associated thermal anomaly fitting

https://doi.org/10.5194/egusphere-2025-5460
Preprint. Discussion started: 24 November 2025

curves. On November 1, 2019, thermal anomalies were predominantly distributed south of the orogenic zone, with greater intensity observed in the southeast compared to the southwest. By November 9, 2019, anomalies were distributed bilaterally across the orogenic zone, with high-value regions exhibiting relatively even distribution. Applying the same analytical method to the Himalayan orogen thermal anomalies revealed a spatial trend subparallel to the orogen's near east-west orientation. The corresponding correlation coefficients (0.9763 and 0.9859) demonstrate a strong positive linear correlation between the Himalayan orogen and its thermal anomalies, according to Pearson's metric. Comparing the correlation coefficients for Dingmu Co Fault (mean = 0.9969) and the Himalayan orogen (mean = 0.9811) reveals a slightly higher average correlation for the fault region. Nevertheless, the extremely high correlation coefficients and the spatial alignment of the anomaly fitting curves with both Dingmu Co Fault and the Himalayan orogen confirm a significant spatial correlation between the thermal anomaly regions and these major geological structures.

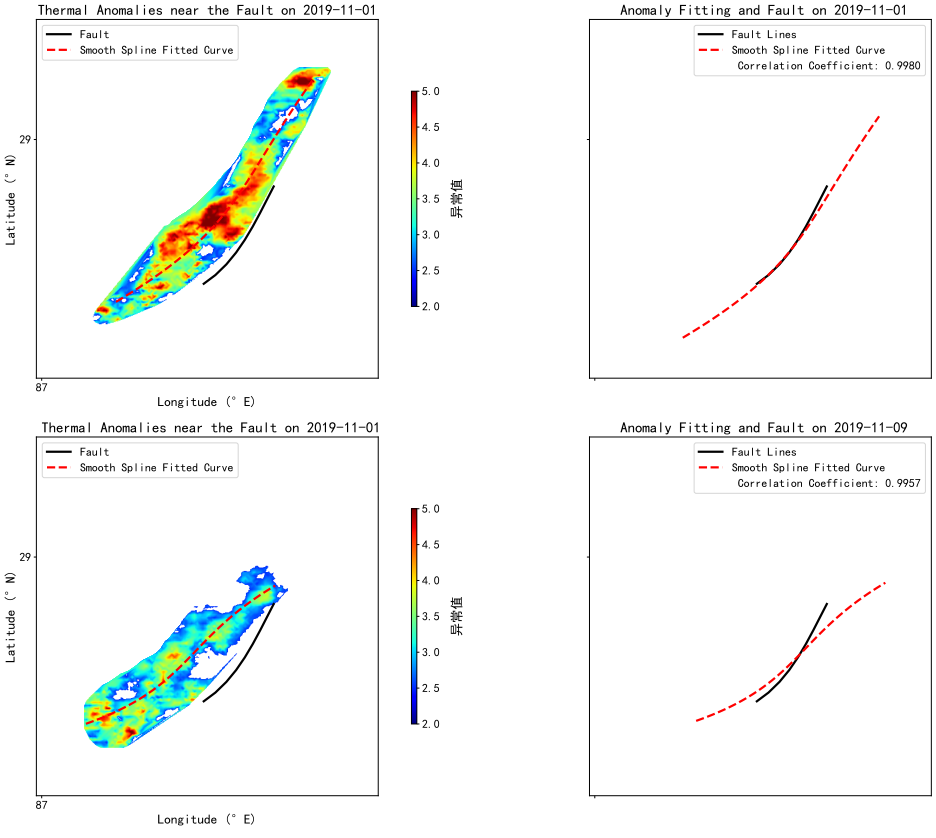

Figure 5. Spatial Relationship Between Thermal Anomalies of the Dingri Ms5.9 Earthquake, Tibet and Dingmu Co Fault (The left figure illustrates the thermal anomalies and fitting curves in Dingmu Co Fault area on November 1 and 9, 2019, along with Dingmu Co Fault. The right figure presents a comparative display of the spatial relationship between the shifted fitting curves and Dingmu Co Fault, as well as their correlation coefficients)

https://doi.org/10.5194/egusphere-2025-5460
Preprint. Discussion started: 24 November 2025

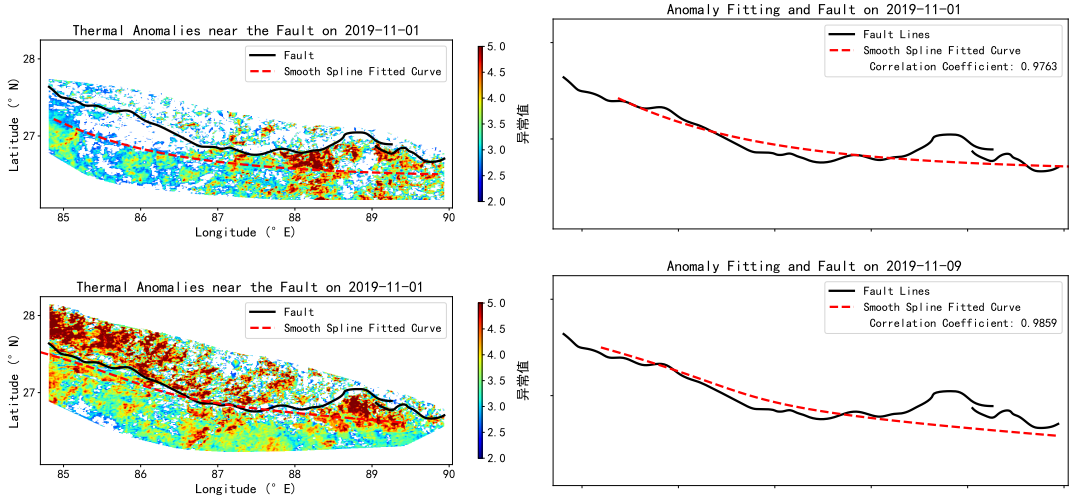

Figure 6. Spatial Relationship Between Thermal Anomalies of the Ms5.9 Dingri Earthquake,Tibet and the Himalayan Orogeny Zone (The left figure illustrates the thermal anomalies, fitting curves, and the Himalayan orogeny zone in the region on 1 and 9 November 2019. The right figure presents a comparative display of the spatial relationship between the shifted fitting curves and the Himalayan orogeny zone, as well as their correlation coefficients)

5.4 Seismicity Analogy Analysis in the Same Region

Comparative analysis of earthquakes within the same region is essential for identifying seismic thermal anomalies and developing refined discrimination indicators to effectively exclude thermally anomalous variations attributable to non-seismic factors. This study conducts a comparative analysis of the 7 January 2025 Dingri Ms6.8 earthquake and the present event, whose epicenters are separated by approximately 13.5 km, using identical data processing methodologies. The resultant spatio-temporal distribution of seismic thermal anomalies is presented in Figure 7. The spatio-temporal evolution exhibits the following progression: From 4 to 11 July 2024, sporadic anomalies emerged south of the epicenter, distinctly clustered adjacent to the fault. During 12 July to 12 August 2024, anomalies migrated progressively toward the epicenter with initial intensification followed by weakening. From 13 August to 5 September 2024, low-intensity anomalies persisted primarily along the fault south of the epicenter. The period 6 to 13 September 2024 featured large-scale, high-intensity banded anomalies distinctly clustered adjacent to the fault, followed by contraction, dispersion, and weakening of anomalies from 14 September to 23 October 2024. Subsequently, 24 October to 16 November 2024 exhibited large-scale, high-intensity anomalies distributed along the fault, while 17 November to 27 December 2024 showed only sporadic low-intensity anomalies. High-intensity, widely distributed anomalies appeared north and east of the epicenter during 1 to 8 January 2025, potentially caused by frictional heating during coseismic crustal rupture. Anomalies returned to sporadic low-intensity states from 9 January to 1 February 2025. Subsequently, newly emerged anomalies reappeared during 2 to 9 February 2025, potentially linked to persistent aftershock activity following the mainshock.

https://doi.org/10.5194/egusphere-2025-5460
Preprint. Discussion started: 24 November 2025

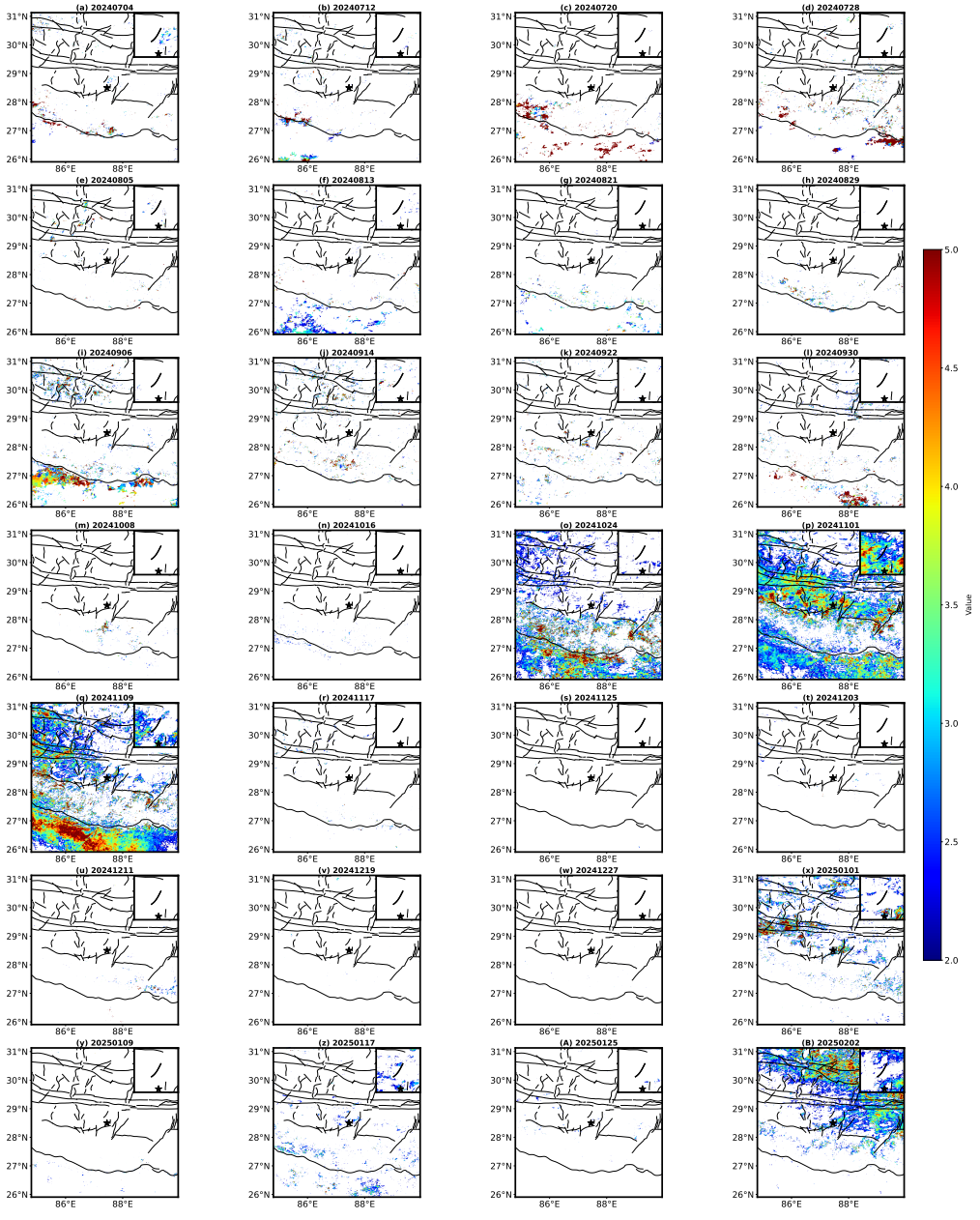

Figure 7. Similar to Figure 3. Spatiotemporal Distribution of Thermal Anomalies with the 7 January 2025 Ms6.8 Dingri Earthquake, Tibet

https://doi.org/10.5194/egusphere-2025-5460
Preprint. Discussion started: 24 November 2025

Figure 8 illustrates the temporal variations in thermal anomaly pixel counts within the study area from 4 July 2024 to 2 February 2025, with comparisons made against the corresponding multi-year average from non-seismic periods. Analysis indicates that pronounced fluctuations occurred during the six-month pre-seismic phase preceding the Dingri Ms 6.8 earthquake in Tibet. Between July and mid-October 2024, pixel counts remained consistently low, showing only minor deviations from the non-seismic baseline. A noticeable increase commenced in late October 2024, culminating in a peak of 450,000 pixels on 1 November—significantly exceeding the multi-year average and suggesting a clear pre-seismic anomaly. The values then decreased gradually over approximately 24 days. From 17 November 2024 until the mainshock, no notable thermal anomalies were detected. Following the earthquake, fluctuations of varying magnitudes were observed. It is noteworthy that the Dingri Ms 6.8 earthquake occurred 67 days after the thermal anomaly peak.

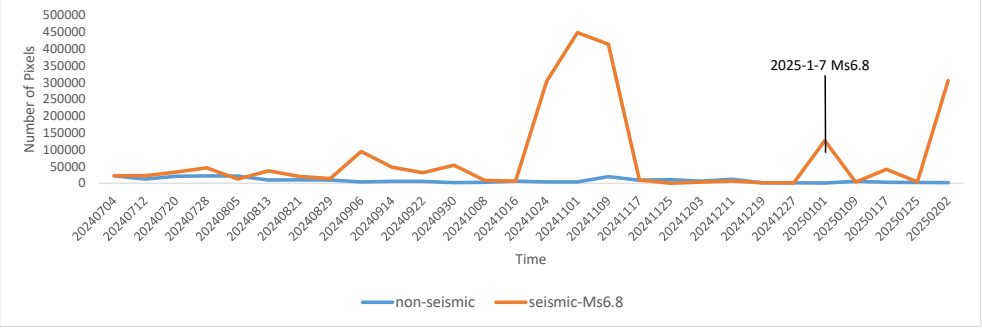

Figure 8. Similar to Figure 4. Temporal evolution of thermal anomalies: Ms6.8 Dingri earthquake, Tibet(7 January 2025)

During our investigation of the 20 March 2020 Dingri Ms5.9 earthquake in Tibet, a significant spatial correlation between thermal anomalies and fault structures within Dingmu Co Fault zone and the Himalayan orogenic belt was identified. To validate this correlation for the current event, we applied identical methodology to analyze thermal anomaly regions associated with these structures. Figure 9 illustrates the spatial relationship between Dingmu Co Fault and fitted curves derived from proximal thermal anomalies. On 1 November 2024, anomalies were distributed northwest of the fault, exhibiting higher values south of the fault compared to northern areas. On 9 November 2024, anomalies remained northwest of the fault with higher-value clusters predominantly south of the structure. Post-fitting and shifting procedures yielded fitted curves demonstrating close alignment with Dingmu Co Fault, both exhibiting near-identical north-south strike orientations. Calculated Pearson correlation coefficients of 0.9973 and 0.9965 confirm an exceptionally strong correlation. Figure 10 presents the spatial relationship between the Himalayan orogenic belt and corresponding fitted curves. On 24 October 2024, anomalies were symmetrically distributed across both sides of the orogen. On 1 November 2024, anomalies shifted predominantly southward with higher-value concentrations in the eastern sector. On 9 November 2024, anomalies occurred bilaterally but with greater density south of the orogen and higher-value clusters in the western sector. Resultant fitted curves after processing align subparallel to the

https://doi.org/10.5194/egusphere-2025-5460
Preprint. Discussion started: 24 November 2025

orogen's near east-west strike direction. Correlation coefficients of 0.9876, 0.9582, and 0.9661 indicate strong correlation, albeit comparatively lower than those observed for Dingmu Co Fault region. Unlike the previous event, the thermal anomalies in this case exhibited a certain spatial offset from the surface trace of the fault zone. Although distantly located from the primary fault, these anomalies may be situated within the boundary zone of the same large-scale tectonic block or associated with activity along deep-seated blind faults. During the late stage of earthquake preparation, the crustal stress-strain field undergoes adjustments across an extensive region—termed the "seismogenic system"—which may generate thermal anomalies at specific locations distant from the main fault through various mechanisms (e.g., stress transfer, pore pressure variations, charge carrier transport). Consequently, the "spatial correlation" we refer to should not be interpreted as requiring strict alignment along the fault trace, but rather understood as a correlation with the entire "seismogenic tectonic system," rather than solely with a single surface rupture line.

Comparative analysis of seismic events within the same tectonic region enables effective filtering of interference from geological, atmospheric, and geographical factors, thereby enhancing the reliability of thermal anomaly prediction indicators. The proximate epicenters and identical focal depths of these two earthquakes yielded comparable thermal anomaly characteristics: distinct thermal anomalies emerged within their respective six-month pre-seismic periods, predominantly concentrated near major faults. Spatial distributions at peak anomaly intensity demonstrated similar patterns, with concentrations along identical tectonic structures (Dingmu Co Fault and the Himalayan orogenic belt). Notably, thermal anomaly regions exhibited statistically significant spatial correlations with both Dingmu Co Fault and the Himalayan orogenic belt. These consistent patterns provide critical references for identifying region-specific thermal anomalies. The observed seismic characteristic homogeneity likely reflects inherent physical properties of this tectonically active region.

6 Temporal Variation Characteristics of Earthquake Thermal Infrared Periods

To explore seismic thermal infrared anomalies in the study area, we used the empirical relation $R_D = 10^{0.43M}$ (where M is the earthquake magnitude) proposed by previous researchersDobrovolsky et al. (1979). Earthquakes of magnitude $\geq$4.0 occurring between January 2016 and February 2025 were selected for analysis. For the 20 March 2020 Dingri Ms5.9 earthquake (epicenter: 87.42°E, 28.63°N), a circular study area (radius = 52.5 km) was defined. A total of 22 earthquakes were recorded within this zone (Table 1). Time-series analysis (Figure 11) revealed that the anomaly index in Period A exceeded 1 approximately three months prior to the earthquake (22 May 2016). This elevated index persisted for about one month before gradually decreasing. A brief increase in the anomaly index was observed again during mid-to-late April. However, in the period immediately preceding the seismic event, the anomaly index remained consistently low. In Period B, a sustained anomaly lasting 16 days emerged from late April to early May 2019. Following this, the anomaly index remained below 1. From late June to late September, it fluctuated repeatedly. On 1 November, the index surged abruptly before plummeting. Subsequently, it continued to fluctuate until the earthquake occurred on 20 March 2020. In Period C, oscillations approaching 1.5 began approximately seven months prior to the occurrence of two earthquakes in early February 2021. In Period D, an anomaly index exceeding 1 was observed one month before the earthquake that occurred on 5 November 2021. In Period E, anomalies with an anomaly

https://doi.org/10.5194/egusphere-2025-5460
Preprint. Discussion started: 24 November 2025

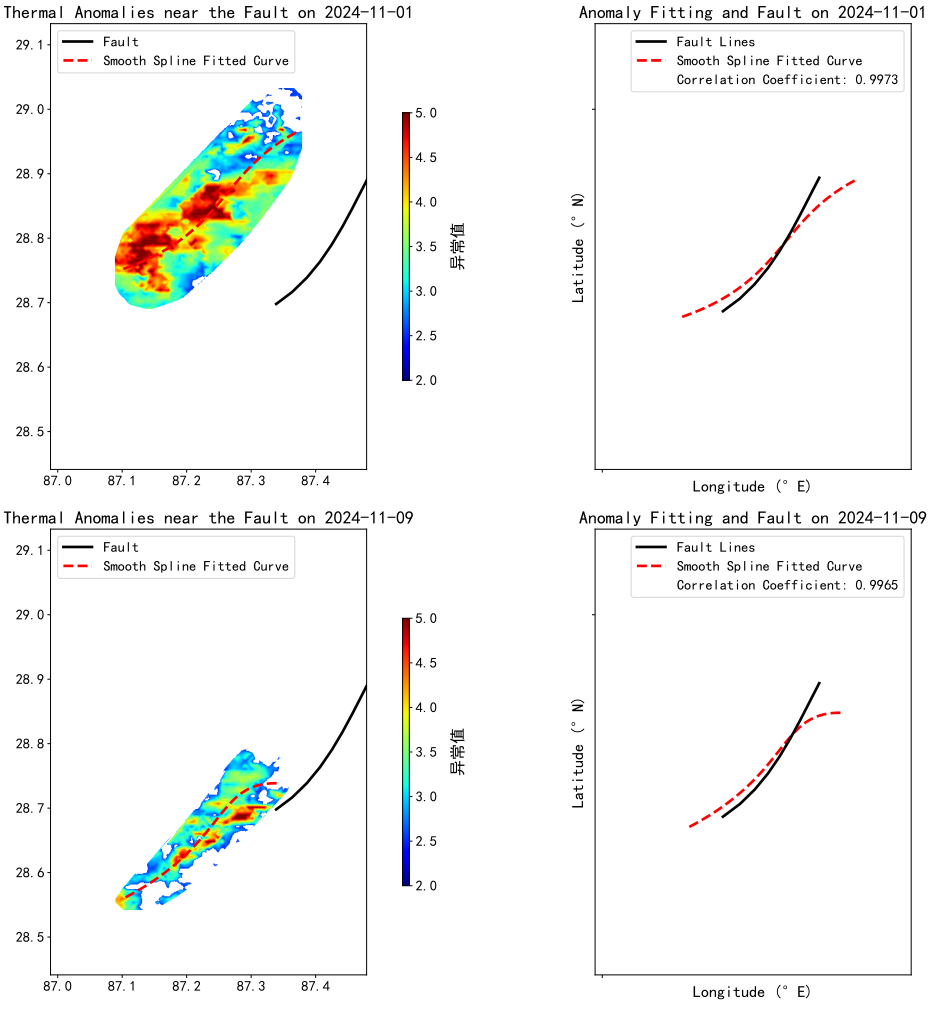

Figure 9. Similar to Figure 5. Spatial Relationship Between Thermal Anomalies of the Dingri Ms6.8 Earthquake, Tibet and Dingmu Co Fault

https://doi.org/10.5194/egusphere-2025-5460
Preprint. Discussion started: 24 November 2025

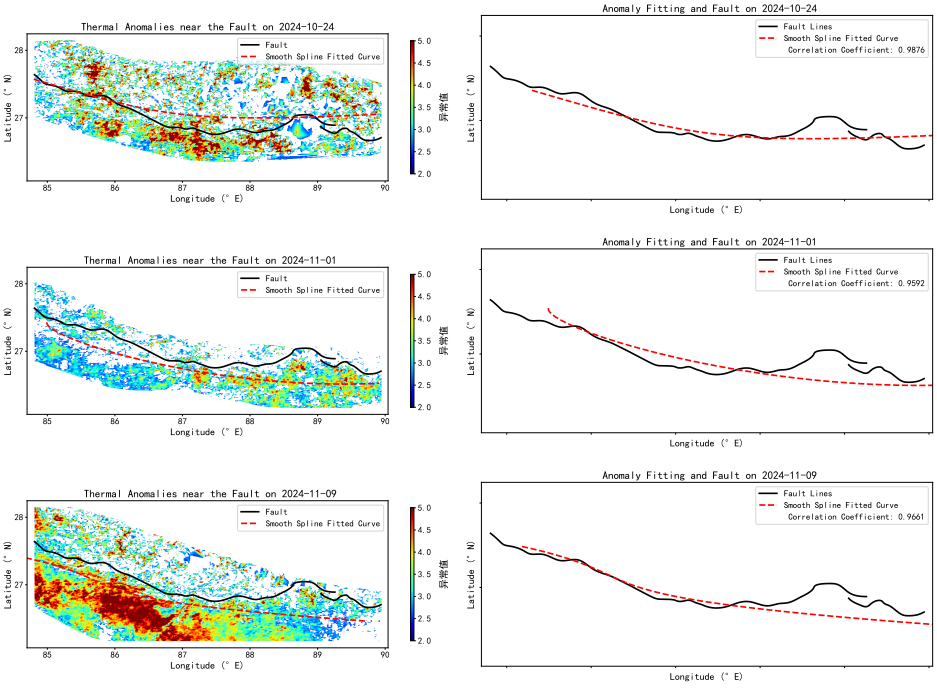

Figure 10. Similar to Figure 6. Spatial Relationship Between Thermal Anomalies of the Dingri Ms6.8 Earthquake, Tibet and the Himalayan Orogeny Zone

index exceeding 2 occurred once each in late April and late May 2024, prior to the main shock on 7 January 2025 and its subsequent aftershocks. A period of persistently high anomaly index re-emerged in late October, lasting for 24 days. However, from mid-to-late November onwards and persisting until immediately before the main shock, the anomaly index remained consistently low. Following the main shock on 7 January 2025, the index resumed increasing. This phenomenon may be associated with the incomplete release of crustal stress, a notion corroborated by the occurrence of aftershocks after the main shock.

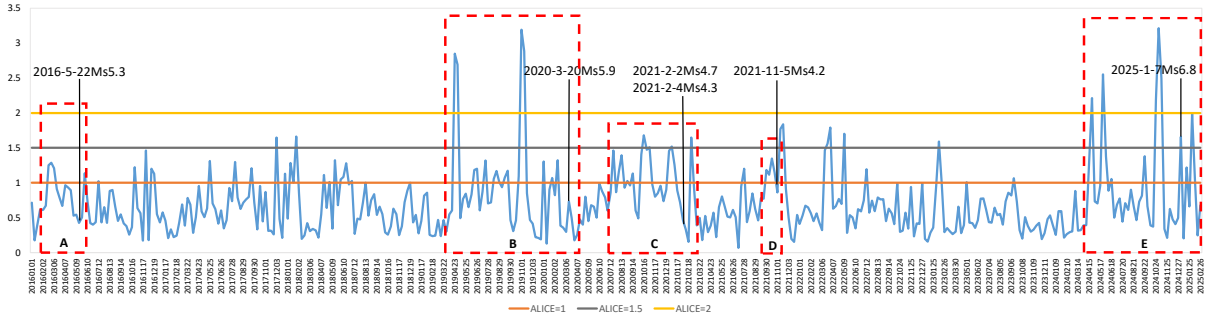

Figure 11. Correspondence diagram of regional thermal anomaly index time series and earthquakes

https://doi.org/10.5194/egusphere-2025-5460
Preprint. Discussion started: 24 November 2025

Table 1. Catalogue of earthquakes with Ms≥ 4.0 in the region

Period	Date	Epicenter	Magnitude (Ms)	Anomaly Onset	Anomaly Peak Interval	Anomaly Amplitude
A	2016-05-22	28.31°N, 87.62°E	4.1	3 months before	86 days	Index > 1
		28.36°N, 87.60°E	5.3			
		28.41°N, 87.59°E	5.3			
		28.59°N, 87.50°E	4.1			
B	2020-03-20	28.63°N, 87.42°E	5.9	11 months before	140 days	Index > 2
C	2021-02-02	28.55°N, 87.50°E	4.7	7 months before	109 days	Index > 1.5
		28.64°N, 87.52°E	4.3		111 days	
D	2021-11-05	28.73°N, 87.44°E	4.2	1 month before	20 days	Index > 1
E	2025-01-07	28.50°N, 87.45°E	6.8	9 months before	67 days	Index > 2
		28.35°N, 87.37°E	4.4			
		28.36°N, 87.67°E	4.2			
	2025-01-08	28.22°N, 87.63°E	4.1			
		28.42°N, 87.44°E	4.9			
		28.42°N, 87.50°E	4.9			
	2025-01-13	28.45°N, 87.52°E	5.0			
		28.47°N, 87.50°E	4.2			
	2025-01-16	28.47°N, 87.50°E	4.4			
	2025-01-18	28.35°N, 87.57°E	4.6			
	2025-01-19	28.36°N, 87.57°E	4.2			
		28.20°N, 87.56°E	4.6			
	2025-01-21	28.28°N, 87.54°E	4.1			
	2025-01-27	28.38°N, 87.51°E	4.1			

7 Discussion

This study reveals a robust correlation between thermal anomalies and faults during the Dingri earthquake, Tibet, a finding of significant importance for understanding thermal anomaly phenomena in the earthquake preparation process. Through processing MODIS data using the STL time-series decomposition method and the RST algorithm, we identified that the spatial distribution of thermal anomalies exhibits a high degree of correspondence with Dingmu Co Fault and the Himalayan orogenic belt. This robust correlation indicates that faults play a critical role in the formation and evolution of seismic thermal anomalies, providing a key perspective for understanding thermal anomaly phenomena during earthquake preparation. The mechanistic analysis for this observed strong correlation is illustrated in Figure 12 below.

The formation of surface thermal anomalies during the earthquake gestation process is a complex process involving the coupling of multiple physical mechanisms. The core driving force originates from the continuous accumulation of crustal stress.

https://doi.org/10.5194/egusphere-2025-5460
Preprint. Discussion started: 24 November 2025

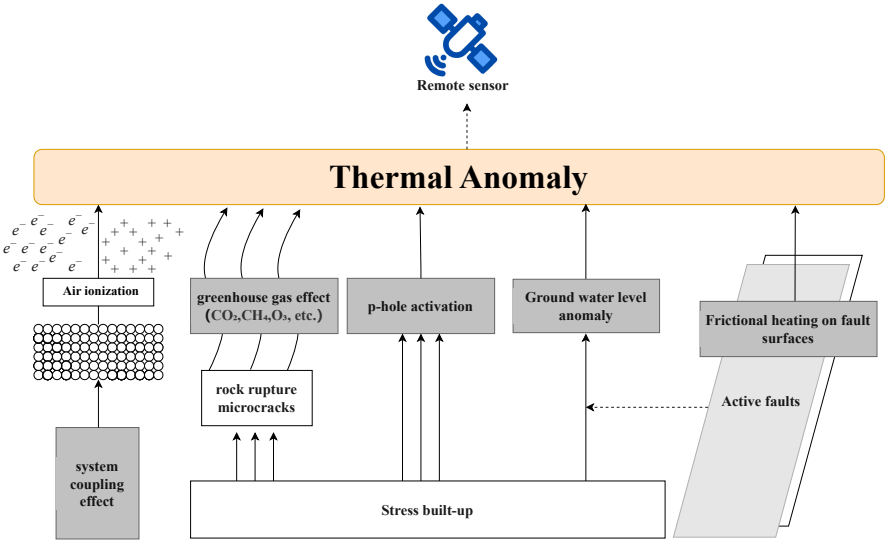

Figure 12. Introduction to Pre-seismic Thermal Anomaly Mechanisms(Crustal stress accumulation induces rock fracturing with consequent micro-crack generation, facilitating the release of trapped or deep-sourced greenhouse gases (CO_2, CH_4, etc.). Crustal stress accumulation concurrently activates positive hole (p-hole) charge carrier activity . fault motion generates frictional heating along fault planes. Under coupled system effects, ionization may occur in near-surface atmospheres. Furthermore, stress perturbations significantly modify groundwater dynamics, inducing anomalous hydraulic fluctuations. Through synergistic integration of these mechanisms, detectable surface thermal anomalies may ultimately manifest and be captured by thermal infrared remote sensing instruments.)

As the stress level approaches the rock fracture threshold, microcracks are induced to nucleate and propagate. The continuous evolution and interconnection of the microcrack network ultimately lead to macroscopic rupture, a process that is accompanied by the release of greenhouse gases, which may contribute to local thermal effectsSun et al. (2021). The accumulation of stress also activates p-holes (positive charge vacancies) within the rocks. The activated p-holes migrate through the crystal lattice and release heat through redox reactions with surrounding materials, forming a heat flux that enhances surface thermal infrared radiationOuzounov and Freund (2004). The earthquake gestation process also significantly disturbs the subsurface fluid system. Fault activity alters the seepage pathways of groundwater, causing abnormal water level fluctuations (either rising or falling), which directly interfere with the thermal state and heat transfer processes of groundwaterChen et al. (2013). This, in turn, leads to the redistribution of the shallow geothermal field and is reflected in the surface thermal radiation signal. Among various heat-generating mechanisms, the frictional heat generated by the relative motion of the fault blocks is particularly critical. The substantial amount of heat produced not only significantly raises the temperature near the fault zone but also efficiently conducts to the surface through preferential pathways within the fault breccia (such as fractures and pores)Rattez and Veveakis (2020); Ouzounov et al. (2007). It is noteworthy that, given the large-scale characteristics of the thermal anomalies and their spatial distribution controlled by fault structures, we have reason to believe that fault frictional heating is likely a key potential

https://doi.org/10.5194/egusphere-2025-5460
Preprint. Discussion started: 24 November 2025

factor. Furthermore, the coupling effects between the lithosphere, hydrosphere, and atmosphere are also significant factors during the earthquake preparation process. The interaction between deep processes and shallow/surface environments may induce near-surface air ionization, generating a large number of free electrons. The inelastic collisions of free electrons with gas molecules can lead to local gas warming. Meanwhile, the space charge generated by ionization can modulate the infrared emissivity of surface objects, collectively affecting the intensity of thermal anomaliesWu et al. (2023a); Pulinets and Dunajecka (2007).

The presence of thermal anomalies points to possible intense tectonic activity or stress accumulation in the region. It should be understood, however, that not all stress accumulation culminates in an earthquake; specific critical conditions, including the Coulomb failure criterion, must be met. Anomalies observed in other areas could reflect processes such as subcritical crustal creep, aseismic slip, or alternative energy release mechanisms. The interpretation of the studied anomalies as precursors is based on their prominent spatiotemporal association with the earthquake and their marked spatial correspondence with the known seismogenic fault. Acknowledging that the absence of continuous InSAR deformation data precluded direct cross-validation in this study, addressing this gap will be a central aim of subsequent research. Integration of such data is crucial for elucidating the physical relationship between thermal anomalies and fault activity.

In summary, pre-earthquake thermal anomalies are the result of the combined influence of multiple potential mechanisms. Our research reveals a distinct fault-controlled distribution pattern of thermal anomalies, as evidenced by spatial correlation analysis. Considering the scale characteristics and spatial control of the thermal anomalies, we believe that fault frictional heating is more likely to be the key potential factor compared to other potential mechanisms. These coupling processes, centered on fault activity, collectively lead to the thermal anomalies distributed along the fault in the earthquake gestation area. This spatial correlation provides important physical evidence for using satellite remote sensing technology to monitor fault activity and explore earthquake prediction.

8 Conclusions

This study utilized the STL time series decomposition method to remove trend and seasonal components from MOD11A2 data. The residual component was then analyzed using the RST algorithm for anomaly detection, revealing the spatiotemporal evolution characteristics of thermal anomalies before the Ms5.9 Dingri earthquake, Tibe. Significant pre-seismic thermal anomalies were detected, primarily concentrated near fault zones. Investigation of the temporal characteristics of seismic thermal infrared anomalies revealed that the earthquake occurred 140 days after the thermal anomaly peaked, indicating that thermal infrared anomalies can serve as important precursor indicators for seismic activity. Fitting translation analysis was performed on thermal anomaly regions along Dingmu Co Fault and the Himalayan orogenic belt. The results demonstrated a distinct spatial affinity of anomalies to fault structures. Correlation coefficients exceeded 0.99 in Dingmu Co Fault region and 0.95 in the Himalayan orogenic belt region, indicating a strong correlation between thermal anomaly distribution and fault strike. This further confirms the close relationship between thermal infrared anomalies and fault activity. Comparative analysis with the 7 January 2025 Dingri Ms6.8 earthquake revealed similar spatiotemporal characteristics in thermal infrared anomalies. Both events showed

https://doi.org/10.5194/egusphere-2025-5460
Preprint. Discussion started: 24 November 2025

thermal anomalies concentrated near the same faults (Dingmu Co Fault and the Himalayan orogenic belt). Although the exact timing of anomaly appearance differed, significant thermal anomalies preceded both earthquakes. This comparative analysis enhances the credibility of thermal infrared anomalies as predictive indicators and provides more precise discriminative criteria for earthquake prediction. Analysis of the thermal infrared anomaly index time series for Ms≥4.0 earthquakes between 2016 and 2025 showed a significant correlation between anomaly index variations and earthquake occurrence times. This further supports thermal infrared anomalies as important precursor indicators for seismic activity, providing critical information for earthquake prediction. While thermal anomalies may originate from multifactorial sources (e.g., greenhouse gas emissions), we propose that fault friction likely constitutes the dominant mechanism, as evidenced by their large-scale spatial alignment with fault zones. Current constraints in data volume and research capabilities leave key issues unresolved: (1) The temporal pattern between pre-seismic anomaly peak timing and earthquake occurrence; (2) The universality of the observed significant spatial correlation between thermal anomalies and fault zones across different seismic events. Future work should expand datasets with multi-earthquake cases and conduct rigorously designed experiments to investigate the temporal regularity of precursory anomaly peaks and the universality of fault-controlled thermal anomaly distributions.

Code availability. The code generated and used during the current study are not publicly available but are available from the corresponding author on reasonable request

Data availability. Earthquake catalog: China Earthquake Networks Center (http://data.earthquake.cn); Active fault data: China Active Fault Data Center (https://www.activefault-datacenter.cn); Land surface temperature: NASA LAADS (https://ladsweb.modaps.eosdis.nasa.gov/)

Author contributions. Wanyi Li: Conceptualization, Methodology, Software, Formal analysis, Investigation, Resources, Data curation, Writing - original draft, Writing - review and editing, Visualization, Project administration. Dan Tao: Conceptualization, Methodology, Validation, Investigation, Supervision, Writing - review and editing, Project administration, Funding acquisition. Jiufeng Wang: Investigation, Supervision. Xiang Wei: Software, Supervision. Qianxi Zhang: Investigation. Yinqian Li: Data curation. Sirui Li: Supervision. Huaxiang Qin: Data curation. Qifeng Jiang: Data curation.

Competing interests. The authors declare no conflict of interest.

Disclaimer. Publisher's note: Copernicus Publications remains neutral with regard to jurisdictional claims made in the text, pub lished maps, institutional affiliations, or any other geographical rep resentation in this paper. While Copernicus Publications makes ev ery effort to include

https://doi.org/10.5194/egusphere-2025-5460
Preprint. Discussion started: 24 November 2025

appropriate place names, the final responsibil ity lies with the authors. Views expressed in the text are those of the authors and do not necessarily reflect the views of the publisher.

330 *Acknowledgements.* We gratefully acknowledge the financial support for this research provided by the National Natural Science Foundation of China (Grant No. 42004137) and the Natural Science Foundation of Sichuan Province of China (Grant No. 2022NSFSC0213 and 26ZRMS0823)

Financial support. This work is supported by the National Natural Science Foundation of China (Grant No. 42004137); The Natural Science Foundation of Sichuan Province of China (Grant No. 2022NSFSC0213 and 26ZRMS0823)

https://doi.org/10.5194/egusphere-2025-5460
Preprint. Discussion started: 24 November 2025

References

Allison, K. L. and Dunham, E. M.: 1 Influence of Shear Heating and Thermomechanical 2 Coupling on Earthquake Sequences and the 3 Brittle-Ductile Transition, Solid Earth, 2020.

Alvan, H. V., Azad, F. H., and Mansor, S.: Latent Heat Flux and Air Temperature Anomalies along an Active Fault Zone Associated with Recent Iran Earthquakes, Advances in Space Research, 52, 1678–1687, https://doi.org/10.1016/j.asr.2013.08.002, 2013.

Bayram, H., Rastgeldi Dogan, T., Şahin, Ü. A., and Akdis, C. A.: Environmental and Health Hazards by Massive Earthquakes, Allergy, 78, 2081–2084, https://doi.org/10.1111/all.15736, 2023.

Chen, J., Yang, X., Yao, L., Ma, S., and Shimamoto, T.: Frictional and Transport Properties of the 2008 Wenchuan Earthquake Fault Zone: Implications for Coseismic Slip-Weakening Mechanisms, Tectonophysics, 603, 237–256, https://doi.org/10.1016/j.tecto.2013.05.035, 2013.

Choudhury, S., Dasgupta, S., Saraf, A. K., and Panda, S.: Remote Sensing Observations of Pre-earthquake Thermal Anomalies in Iran, International Journal of Remote Sensing, 27, 4381–4396, https://doi.org/10.1080/01431160600851827, 2006.

Cicerone, R. D., Ebel, J. E., and Britton, J.: A Systematic Compilation of Earthquake Precursors, Tectonophysics, 476, 371–396, https://doi.org/10.1016/j.tecto.2009.06.008, 2009.

Cleveland, R. B., Cleveland, W. S., McRae, J. E., and Terpenning, I.: STL: A Seasonal-Trend Decomposition Procedure Based on LOESS, Journal of Official Statistics, Vol. 6, 373, 1990.

De Santis, A., Perrone, L., Calcara, M., Campuzano, S., Cianchini, G., D'Arcangelo, S., Di Mauro, D., Marchetti, D., Nardi, A., Orlando, M., Piscini, A., Sabbagh, D., and Soldani, M.: A Comprehensive Multiparametric and Multilayer Approach to Study the Preparation Phase of Large Earthquakes from Ground to Space: The Case Study of the June 15 2019, M7.2 Kermadec Islands (New Zealand) Earthquake, Remote Sensing of Environment, 283, 113 325, https://doi.org/10.1016/j.rse.2022.113325, 2022.

Dobrovolsky, I. P., Zubkov, S. I., and Miachkin, V. I.: Estimation of the Size of Earthquake Preparation Zones, pure and applied geophysics, 117, 1025–1044, https://doi.org/10.1007/bf00876083, 1979.

Freund, F.: Pre-Earthquake Signals: Underlying Physical Processes, Journal of Asian Earth Sciences, 41, 383–400, https://doi.org/10.1016/j.jseaes.2010.03.009, 2011.

Freund, F. T., Takeuchi, A., and Lau, B. W.: Electric Currents Streaming out of Stressed Igneous Rocks – A Step towards Understanding Pre-Earthquake Low Frequency EM Emissions, Physics and Chemistry of the Earth, Parts A/B/C, 31, 389–396, https://doi.org/10.1016/j.pce.2006.02.027, 2006.

Freund, F. T., Takeuchi, A., Lau, B. W. S., Al-Manaseer, A., Fu, C. C., Bryant, N. A., and Ouzounov, D.: Stimulated Infrared Emission from Rocks: Assessing a Stress Indicator, 2007.

Geller, R. J., Jackson, D. D., Kagan, Y. Y., and Mulargia, F.: Earthquakes Cannot Be Predicted, Science, 275, 1616–1616, https://doi.org/10.1126/science.275.5306.1616, 1997.

Ghamry, E., Mohamed, E. K., Abdalzaher, M. S., Elwekeil, M., Marchetti, D., De Santis, A., Hegy, M., Yoshikawa, A., and Fathy, A.: Integrating Pre-Earthquake Signatures From Different Precursor Tools, IEEE access : practical innovations, open solutions, 9, 33 268–33 283, https://doi.org/10.1109/ACCESS.2021.3060348, 2021.

Gorny, V., Salman, A., Tronin, A. A., and Shilin, B.: Gorny-1988-The Earth's Outgoing IR Radiation as an Indicator of Seismic Activity, Proceedings of the Academy of Sciences of the USSR, 301, 67–69, 1988.

https://doi.org/10.5194/egusphere-2025-5460
Preprint. Discussion started: 24 November 2025

Hassini, A. and Belbachir, A. H.: Thermal Method of Remote Sensing for Prediction and Monitoring Earthquake, in: 2014 1st International Conference on Information and Communication Technologies for Disaster Management (ICT-DM), pp. 1–6, IEEE, Algiers, Algeria, ISBN 978-1-4799-4767-6 978-1-4799-4768-3, https://doi.org/10.1109/ICT-DM.2014.6917790, 2014.

Hill, E. M., McCaughey, J. W., Switzer, A. D., Lallemant, D., Wang, Y., and Sathiakumar, S.: Human Amplification of Secondary Earthquake Hazards through Environmental Modifications, Nature Reviews Earth & Environment, 5, 463–476, https://doi.org/10.1038/s43017-024-00551-z, 2024.

Jiang, M., Jing, F., and Zhang, L.: Evaluating Multiparameter Response to Seismic Thermal Anomalies From Global Major Earthquakes, IEEE Journal of Selected Topics in Applied Earth Observations and Remote Sensing, 18, 11 835–11 850, https://doi.org/10.1109/JSTARS.2025.3563992, 2025.

Jiao, Z.-H., Zhao, J., and Shan, X.: Pre-Seismic Thermal Anomalies from Satellite Observations: AReview, https://doi.org/10.5194/nhess-2017-211, 2017.

Jin, Z., Zhou, M., Huang, J., and Wan, Y.: The Stress Triggering of the 2025 Dingri, Xizang, China MW6.8 Earthquake by the 2015 Nepal MW7.8 and MW7.2 Earthquakes(In Chinese), Earth Science-Journal of China University of Geosciences, 50, 1782–1793, https://doi.org/10.3799/dqkx.2025.074, 2025.

Jing, F., Singh, R. P., and Shen, X.: Land – Atmosphere – Meteorological Coupling Associated with the 2015 Gorkha (M 7.8) and Dolakha (M 7.3) Nepal Earthquakes, Geomatics, Natural Hazards and Risk, 10, 1267–1284, https://doi.org/10.1080/19475705.2019.1573629, 2019.

Kancherla, V. K., Mandla, V. R., and Arrowsmith, C.: Study of Thermal IR Phenomena Associated with 27 February 2010 Chile Mw 8.8 Earthquake Using MODIS Data, Geocarto International, 33, 293–309, https://doi.org/10.1080/10106049.2016.1250824, 2018.

Karimi Zarchi, A. and Saradjian Maralan, M. R.: Fault Distance-Based Approach in Thermal Anomalydetection before Strong Earthquakes, https://doi.org/10.5194/nhess-2020-391, 2020.

Koronovskii, N. V., Zakharov, V. S., and Naimark, A. A.: The Unpredictability of Strong Earthquakes: New Understanding and Solution of the Problem, Moscow University Geology Bulletin, 76, 366–373, https://doi.org/10.3103/S0145875221040074, 2021.

Lai, Z., Chao, J., Zhao, Z., Wen, M., Yang, H., Chai, W., Yao, Y., Zhao, X., Chen, Q., and Liu, J.: Relationship between Crustal Deformation and Thermal Anomalies in the 2022 Ninglang Ms 5.5 Earthquake in China: Clues from InSAR and RST, Remote Sensing, 15, 1271, https://doi.org/10.3390/rs15051271, 2023.

Li, Q., Li, C., Zhao, B., Huang, Y., Wan, Y., Tan, K., and Dong, Q.: Estimated Seismic Source Parameters for the 2020 Dingri MW5.6 Earthquake in Xizang and Study on the Stress Triggering(In Chinese), Chinese Journal of Geophysics, 67, 172–188, https://doi.org/10.6038/cjg2022Q0234, 2024.

Liu, P., Chen, S., Liu, Q., Guo, Y., Ren, Y., Zhuo, Y., and Feng, J.: A Potential Mechanism of the Satellite Thermal Infrared Seismic Anomaly Based on Change in Temperature Caused by Stress Variation: Theoretical, Experimental and Field Investigations, Remote Sensing, 14, 5697, https://doi.org/10.3390/rs14225697, 2022.

Liu, S., Xu, Z., Wei, J., Huang, J., and Wu, L.: Experimental Study on Microwave Radiation From Deforming and Fracturing Rock Under Loading Outdoor, IEEE Transactions on Geoscience and Remote Sensing, 54, 5578–5587, https://doi.org/10.1109/TGRS.2016.2569419, 2016.

Marchetti, D., De Santis, A., D'Arcangelo, S., Poggio, F., Piscini, A., A. Campuzano, S., and De Carvalho, W. V.: Pre-Earthquake Chain Processes Detected from Ground to Satellite Altitude in Preparation of the 2016–2017 Seismic Sequence in Central Italy, Remote Sensing of Environment, 229, 93–99, https://doi.org/10.1016/j.rse.2019.04.033, 2019.

https://doi.org/10.5194/egusphere-2025-5460
Preprint. Discussion started: 24 November 2025

Ouzounov, D. and Freund, F.: Mid-Infrared Emission Prior to Strong Earthquakes Analyzed by Remote Sensing Data, Advances in Space Research, 33, 268–273, https://doi.org/10.1016/s0273-1177(03)00486-1, 2004.

Ouzounov, D., Liu, D., Chunli, K., Cervone, G., Kafatos, M., and Taylor, P.: Outgoing Long Wave Radiation Variability from IR Satellite Data Prior to Major Earthquakes, Tectonophysics, 431, 211–220, https://doi.org/10.1016/j.tecto.2006.05.042, 2007.

Panda, S. K., Choudhury, S., Saraf, A. K., and Das, J. D.: MODIS Land Surface Temperature Data Detects Thermal Anomaly Preceding 8 October 2005 Kashmir Earthquake, International Journal of Remote Sensing, 28, 4587–4596, https://doi.org/10.1080/01431160701244906, 2007.

Pulinets, S. and Dunajecka, M.: Specific Variations of Air Temperature and Relative Humidity around the Time of Michoacan Earthquake M8.1 Sept. 19, 1985 as a Possible Indicator of Interaction between Tectonic Plates, Tectonophysics, 431, 221–230, https://doi.org/10.1016/j.tecto.2006.05.044, 2007.

Pulinets, S., Ouzounov, D., Karelin, A., Boyarchuk, K., and Pokhmelnykh, L.: The Physical Nature of Thermal Anomalies Observed before Strong Earthquakes, Physics and Chemistry of the Earth, Parts A/B/C, 31, 143–153, https://doi.org/10.1016/j.pce.2006.02.042, 2006.

Rattez, H. and Veveakis, M.: Weak Phases Production and Heat Generation Control Fault Friction during Seismic Slip, Nature Communications, 11, https://doi.org/10.1038/s41467-019-14252-5, 2020.

Rawat, V., Saraf, A. K., Das, J., Sharma, K., and Shujat, Y.: Anomalous Land Surface Temperature and Outgoing Long-Wave Radiation Observations Prior to Earthquakes in India and Romania, Natural Hazards, 59, 33–46, https://doi.org/10.1007/s11069-011-9736-5, 2011.

Reid, H. F.: The California Earthquake of April 18, 1906., Nature, Vol. 84, 166, 1910.

Rogers, G. and Dragert, H.: Episodic Tremor and Slip on the Cascadia Subduction Zone: The Chatter of Silent Slip, Science, 300, 1942–1943, https://doi.org/10.1126/science.1084783, 2003.

Saradjian, M. R. and Akhoondzadeh, M.: Thermal Anomalies Detection before Strong Earthquakes (<I>M</I> > 6.0) Using Interquartile, Wavelet and Kalman Filter Methods, Natural Hazards and Earth System Sciences, 11, 1099–1108, https://doi.org/10.5194/nhess-11-1099-2011, 2011.

Saraf, A. K.: Detecting Earthquake Precursor: A Thermal Remote Sensing Approach, in: Map India-2008: GIS Development, 2008.

Saraf, A. K., Rawat, V., Banerjee, P., Choudhury, S., Panda, S. K., Dasgupta, S., and Das, J. D.: Satellite Detection of Earthquake Thermal Infrared Precursors in Iran, Natural Hazards, 47, 119–135, https://doi.org/10.1007/s11069-007-9201-7, 2008.

Scholz, C. H.: The Mechanics of Earthquakes and Faulting, Cambridge University Press, 2 edn., ISBN 978-0-521-65223-0 978-0-521-65540-8 978-0-511-81851-6, https://doi.org/10.1017/CBO9780511818516, 2002.

Sun, H., Ma, L., Liu, W., Spearing, A., Han, J., and Fu, Y.: The Response Mechanism of Acoustic and Thermal Effect When Stress Causes Rock Damage, Applied Acoustics, 180, 108 093, https://doi.org/10.1016/j.apacoust.2021.108093, 2021.

Tramutoli, V.: Robust AVHRR Techniques (RAT) for Environmental Monitoring: Theory and Applications, in: Remote Sensing, edited by Cecchi, G. and Zilioli, E., pp. 101–113, Barcelona, Spain, https://doi.org/10.1117/12.332714, 1998.

Tramutoli, V.: From Visual Comparison to Robust Satellite Techniques: 30 Years of Thermal Infrared Satellite Data Analyses for the Study of Earthquakes Preparation Phases, https://doi.org/10.4430/bgta0149, 2015.

Tronin, A. A., Hayakawa, M., and Molchanov, O. A.: Thermal IR Satellite Data Application for Earthquake Research in Japan and China, Journal of Geodynamics, 33, 519–534, https://doi.org/10.1016/S0264-3707(02)00013-3, 2002.

Wei, C., Zhang, Y., Guo, X., Hui, S., Qin, M., and Zhang, Y.: Thermal Infrared Anomalies of Several Strong Earthquakes, The Scientific World Journal, 2013, 208 407, https://doi.org/10.1155/2013/208407, 2013.

https://doi.org/10.5194/egusphere-2025-5460
Preprint. Discussion started: 24 November 2025

Wu, L., Liu, S., Wu, Y., and Wang, C.: Precursors for Rock Fracturing and Failure—Part I: IRR Image Abnormalities, International Journal of Rock Mechanics and Mining Sciences, 43, 473–482, https://doi.org/10.1016/j.ijrmms.2005.09.002, 2006.

Wu, L., Qi, Y., Mao, W., Lu, J., Ding, Y., Peng, B., and Xie, B.: Scrutinizing and Rooting the Multiple Anomalies of Nepal Earthquake Sequence in 2015 with the Deviation–Time–Space Criterion and Homologous Lithosphere–Coversphere–Atmosphere–Ionosphere Coupling Physics, Natural Hazards and Earth System Sciences, 23, 231–249, https://doi.org/10.5194/nhess-23-231-2023, 2023a.

Wu, P., Meng, Q., Zhang, Y., Zhan, C., Allam, M., Zhang, L., and Hu, X.: Coarse-Graining Research of the Thermal Infrared Anomalies before Earthquakes in the Sichuan Area on Google Earth Engine, Frontiers in Earth Science, 11, 1101165, https://doi.org/10.3389/feart.2023.1101165, 2023b.

Yao, Q.-L. and Qiang, Z.-J.: Thermal Infrared Anomalies as a Precursor of Strong Earthquakes in the Distant Future, Natural Hazards, 62, 991–1003, https://doi.org/10.1007/s11069-012-0130-8, 2012.

Zhang, X., Jiang, X., Xue, Y., Yao, Q., Xie, M., Zang, Y., Song, J., Lu, X., YU, C., Wan, Z., and Tian, L.: Summary of the Dingri MS5.9 Earthquake in Tibet on March 20, 2020(In Chinese), Seismological and Geomagnetic Observation and Research, 41, 194–203, https://doi.org/10.3969/j.issn.1003-3246.2020.04.024, 2020.

Zhang, Y. and Meng, Q.: A Statistical Analysis of TIR Anomalies Extracted by RSTs in Relation to an Earthquake in the Sichuan Area Using MODIS LST Data, Natural Hazards and Earth System Sciences, 19, 535–549, https://doi.org/10.5194/nhess-19-535-2019, 2019.